` MicroSCALE Screening Reveals Genetic Modifiers of Therapeutic Response in Melanoma

Kris C. Wood, David J. Konieczkowski, Cory M. Johannessen, Jesse S. Boehm, Pablo Tamayo, Olga B. Botvinnik, Jill P. Mesirov, William C. Hahn, David E. Root, Levi A. Garraway and David M. Sabatini (15 May 2012)
Science Signaling **5** (224), rs4. [DOI: 10.1126/scisignal.2002612]

CANCER

MicroSCALE Screening Reveals Genetic Modifiers of Therapeutic Response in Melanoma

Kris C. Wood,[1,2]* David J. Konieczkowski,[2,3] Cory M. Johannessen,[2,3] Jesse S. Boehm,[2] Pablo Tamayo,[2] Olga B. Botvinnik,[2] Jill P. Mesirov,[2] William C. Hahn,[2,3] David E. Root,[2] Levi A. Garraway,[2,3] David M. Sabatini[1,2,4]*

Cell microarrays are a promising tool for performing large-scale functional genomic screening in mammalian cells at reasonable cost, but owing to technical limitations they have been restricted for use with a narrow range of cell lines and short-term assays. Here, we describe MicroSCALE (Microarrays of Spatially Confined Adhesive Lentiviral Features), a cell microarray–based platform that enables application of this technology to a wide range of cell types and longer-term assays. We used MicroSCALE to uncover kinases that when overexpressed partially desensitized *B-RAF*^{V600E}–mutant melanoma cells to inhibitors of the mitogen-activated protein kinase kinase kinase (MAPKKK) RAF, the MAPKKs MEK1 and 2 (MEK1/2, mitogen-activated protein kinase kinase 1 and 2), mTOR (mammalian target of rapamycin), or PI3K (phosphatidylinositol 3-kinase). These screens indicated that cells treated with inhibitors acting through common mechanisms were affected by a similar profile of overexpressed proteins. In contrast, screens involving inhibitors acting through distinct mechanisms yielded unique profiles, a finding that has potential relevance for small-molecule target identification and combination drugging studies. Further, by integrating large-scale functional screening results with cancer cell line gene expression and pharmacological sensitivity data, we validated the nuclear factor κB pathway as a potential mediator of resistance to MAPK pathway inhibitors. The MicroSCALE platform described here may enable new classes of large-scale, resource-efficient screens that were not previously feasible, including those involving combinations of cell lines, perturbations, and assay outputs or those involving limited numbers of cells and limited or expensive reagents.

INTRODUCTION

Gain- and loss-of-function screens are powerful experimental approaches that can be leveraged to reveal the mechanistic underpinnings of a wide range of mammalian cellular biological processes (*1*–*5*). However, the costs and logistical challenges of current screening techniques restrict the range and extent of their application. These restrictions are particularly evident in large-scale screens involving multiple cell lines, genetic and pharmacological perturbations, or assay outputs, or alternatively in cases where cells, detection reagents, or other material resources are limited. Arrayed screens in multiwell plates can provide discrete, multiplexed measurements in proliferation- and image-based assays, but cost, labor requirements, and the need for specialized screening facilities equipped with appropriate biosafety and fluid-handling equipment limit their deployment (*3*, *5*, *6*). Pooled screening approaches address a number of these limitations and enable the screening of larger numbers of genetic constructs at lower cost (*5*, *7*–*10*). However, pooled screening is incompatible with image-based assays and typically requires large quantities of cells and reagents and libraries of genetic overexpression or knockdown reagents that are barcoded. Further, the scale of tissue culture required for pooled screens may present logistical challenges when large numbers of screens, for example, of many different cell lines or environmental perturbations, are required.

Cell microarrays have the potential to combine the best features of existing screening technologies, such as the assay versatility of multiwell plate–based screening and the high efficiency of pooled screening (*11*–*14*). Cell microarrays consist of hundreds to thousands of distinct genetic reagents printed as individual, microscopic "features" on glass slides, which are then seeded with adherent cells that attach and become treated with the reagent present on each feature (*13*, *15*). In principle, these systems make it possible to perform and analyze many parallel genetic perturbations on a single slide with high screening throughput and low cell and reagent consumption. In practice, although they have been featured in a number of interesting proof-of-concept studies describing variations on the basic cell microarray design with potential applications in several areas of cell biology (*13*, *14*, *16*–*21*), these systems have only rarely been adopted in large-scale screening applications because of several technical limitations (*22*, *23*). Namely, microarrays based on chemically delivered DNA expression plasmids or small interfering RNAs can only be used with cell types that are easily transfectable (for example, human embryonic kidney 293T cells) and with screening assays that are short in duration (typically 1 to 3 days) because of the inefficient and transient nature of nonviral transgene expression (*13*–*15*). Conversely, microarrays based on virally delivered open reading frames (ORFs) or short hairpin RNAs (shRNAs) can stably and efficiently infect a wide range of cell types but require large libraries of concentrated, purified viruses that cannot be prepared in a labor- or time-efficient way with existing methods (*24*). Both formats are further limited because cells tend to migrate away from the features on which they originally land and intermix with cells on neighboring features, an effect that considerably decreases the achievable spatial density of printed features

[1]Whitehead Institute for Biomedical Research, 9 Cambridge Center, Cambridge, MA 02142, USA. [2]Broad Institute of Harvard and Massachusetts Institute of Technology, 7 Cambridge Center, Cambridge, MA 02142, USA. [3]Department of Medical Oncology, Dana-Farber Cancer Institute, Harvard Medical School, 450 Brookline Avenue, Boston, MA 02215, USA. [4]Howard Hughes Medical Institute, Department of Biology, Massachusetts Institute of Technology, 77 Massachusetts Avenue, Cambridge, MA 02139, USA.
*To whom correspondence should be addressed. E-mail: kcwood@alum.mit.edu (K.C.W.); sabatini@wi.mit.edu (D.M.S.)

and the range of cell lines that can be used for screening (*13*, *14*, *24*). Finally, the methods described to date for analyzing cell microarray screening data have required specialized automated microscopy and image processing approaches that, although powerful and technologically impressive, are not widely available (*13*, *22*, *23*, *25*, *26*).

We sought to design a cell microarray platform that is free of the restrictions that have previously limited technologies in this field. Specifically, our goals were to enable stable and selectable transgene expression and longer-term assays (up to ~14 days) in most adherent cell types without regard to differences in infectability or migratory properties. To maximize the practical use of this platform, we also sought to achieve scalable, semiautomated microarray production; stable long-term storage; compatibility with existing lentiviral ORF and shRNA libraries (*3*, *6*, *27*); and quantitative analysis that does not require specialized microscopy and image processing. By incorporating techniques from surface engineering, biochemical separations, and DNA microarray technology, we developed MicroSCALE (Microarrays of Spatially Confined Adhesive Lentiviral Features), a miniaturized screening platform that fulfills each of these criteria. Here, we describe the construction of this platform, its validation, and its application to the systematic discovery of kinases that when overexpressed modify the sensitivity of melanoma cells to a panel of clinically relevant targeted therapies.

RESULTS

Development of the MicroSCALE screening platform

This design of the MicroSCALE system (Fig. 1A) was achieved through a series of technical developments. First, we created a methodology to spatially confine infected cell populations into discrete, densely spaced islands that can be assayed for phenotypes of interest in a manner analogous to that of multiwell plates. Spatial confinement of cells is not feasible on uncoated glass slides because the size and localization of the region of infection adjacent to each printed feature varies substantially from cell line to cell line owing to cell migration away from printed features, leading to irregular and poorly localized regions of infection (fig. S1A). To achieve uniform spatial confinement of cells to printed microarray features, we first coated a glass slide with a material that is resistant to cell adhesion and then printed features in two sequential steps: first with a material that promotes localized cell adhesion and then with individual lentiviruses (directly on top of the printed adhesive regions) (fig. S1B). The resultant surfaces produced stable cell adhesion and infection only within printed areas, resulting in islands of uniform size and shape regardless of the cell line used (Fig. 1B and fig. S1C). We used polyacrylamide hydrogel–coated surfaces as the adhesion-resistant substrate coating and gelatin as the printed cell adhesive material, although other potentially suitable strategies have also been described (*18*, *28*, *29*). We have not observed notable changes in cellular morphology or growth rates on printed gelatin features relative to tissue culture plastic.

Second, we developed a method to achieve consistent and high-efficiency infection of cells adhering to printed lentiviral features. This was essential for all downstream screening applications and requires (i) effective binding of viruses to the array surface and (ii) the use of highly concentrated (high titer) virus preparations. Conventional lentiviral preparations do not permit virus-surface binding because of the presence of serum proteins in viral harvest medium (~10% by volume) (fig. S2A). Moreover, the titer of unconcentrated lentiviral preparations [~5×10^7 IFU (infectious units)/ml] was inadequate to achieve consistent, high rates of infection on printed features across cell lines (fig. S2B).

Current techniques for lentiviral concentration and purification rely on high-speed centrifugation of a small number of samples (<10), a process that is incompatible with the parallel, high-throughput concentration of the hundreds to thousands of distinct lentiviruses that we aimed to use in our platform (*30*). Accordingly, we devised a dual purification and concentration technique that permitted high-throughput, parallel preparation and subsequent printing of hundreds of unique high-titer viruses in a single day. This "polyelectrolyte complexation" method, adapted from a technique originally described by Le Doux *et al.* (*31*), involves the sequential addition of oppositely charged polyelectrolytes to lentiviral supernatants to form a polymer complex that entraps lentiviruses by electrostatic interactions. We pelleted the polymer-virus complex by low-speed centrifugation and mechanically resuspended the pellet in a desired volume of printing buffer to yield a concentrated virus solution ready for printing (fig. S3A). This purification and concentration method can be performed in multiwell plates with a conventional benchtop centrifuge at low speed and reliably yields about 80% recovery of functional virus particles (fig. S3B). Once printed, concentrated lentiviruses efficiently infected cells on MicroSCALE features (Fig. 1B). Further, because all ORF- and shRNA-expressing lentiviruses in our libraries contain mammalian selection markers [blasticidin and

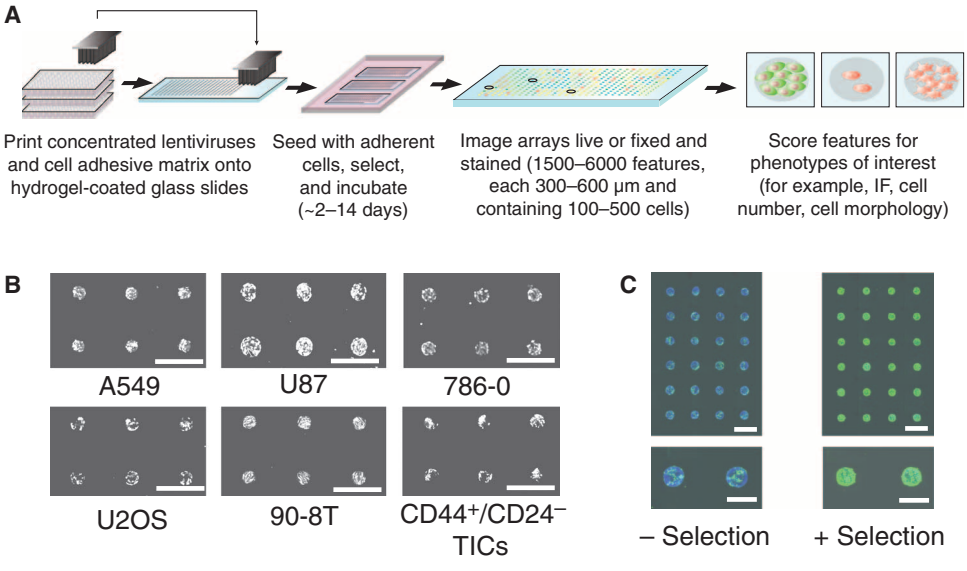

Fig. 1. The MicroSCALE screening platform. (**A**) General schematic depicting screening with MicroSCALE. (**B**) MicroSCALE arrays printed with GFP-expressing lentiviruses were seeded with the indicated cell lines and fixed and imaged after 4 days (GFP fluorescence shown). Scale bar, 1 mm. (**C**) MicroSCALE arrays printed with GFP-expressing lentiviruses were seeded with U2OS cells and incubated for 4 days with (right) or without (left) puromycin selection during days 1 to 4 (blue, Hoechst; green, GFP). Scale bars, 1 mm (top panels) and 500 μm (bottom panels). IF, immunofluorescence; TICs, tumor-initiating cells.

puromycin, respectively (*6*, *32*)], we applied the appropriate selection reagent to ensure that all cells assayed on each feature were stably infected, improving signal resolution by removing uninfected background cells (Fig. 1C and fig. S4). Finally, we used concentrated, printed lentiviruses stored at −80°C over the course of 8 months without observing notable loss of activity.

To test the generality of the MicroSCALE platform using the optimized slide coating and printing processes, we seeded microarrays with a collection of mammalian cell types, including cancer cell lines derived from lung, breast, prostate, skin, brain, pancreas, colon, kidney, liver, and other tissues; genetically engineered, transformed human mammary epithelial cells; and mouse embryonic fibroblasts. Of 32 cell lines tested to date, 27 exhibited efficient adhesion, growth, infection, and selection on MicroSCALE features and are thus deemed suitable for high-throughput screening (tables S1 and S2).

Finally, we developed a simplified approach to quantify MicroSCALE screening results. Automated microscopy, the standard method of analyzing cells on glass slides, can capture complex cellular phenotypes but requires specialized equipment and takes hours to days to analyze the hundreds of features on a single slide (*33*), making it a potentially rate-limiting step for large screens. As an alternative, we found that certain simple, commonly measured phenotypes, such as cell number and phosphoprotein abundance, did not require cellular-level imaging and could be accurately quantified on circular MicroSCALE features by measuring only the total fluorescence intensity on each feature with a conventional DNA microarray scanner (fig. S5). Thus, in applicable screens, this method can analyze an entire slide in minutes, providing a means for rapid analysis of large quantities of screening data.

Applications of the MicroSCALE screening platform

To investigate whether the MicroSCALE platform could reproduce a representative set of proliferation- or staining-based results found by standard multiwell plate–based assays, we performed a series of experiments. First, we verified that proliferation on microscopic features was accurately monitored over time by comparing the effects of control [green fluorescent protein (GFP)–targeted] and cytostatic [polo-like kinase 1 (PLK1)–targeted and casein kinase 1ε (CSNK1E)–targeted] shRNAs, which block mitotic progression (Fig. 2A) (*3*). Second, we reproduced observations concerning oncogene addiction and synthetic lethality, demonstrating the dependence of epidermal growth factor receptor (*EGFR*)–mutant non–small cell lung cancers on growth signaling through EGFR and the related receptor ErbB3 and the dependence of *KRAS*-mutant cancers on both KRAS and TANK-binding kinase 1 (TBK1) (Fig. 2B) (*4*, *34*). Third, by immunofluorescence, we demonstrated that the phosphorylation of ribosomal protein S6 required the upstream activity of mTOR (mammalian target of rapamycin) and Raptor, components of mTOR complex 1 (mTORC1) (Fig. 2C) (*35*).

We also demonstrated that MicroSCALE reliably identified proteins that affected drug sensitivity in a large-scale screen. We focused specifically on kinases because they mediate the activity of diverse cell signaling pathways and may be a rich source of druggable targets that affect drug sensitivity (*32*, *36*). We applied the semiautomated virus concentration and printing techniques described above to produce Kinome ORF MicroSCALEs, each printed with 1632 features consisting of 618 lentivirally delivered ORF constructs printed in duplicate or triplicate (Fig. 2D). The sequence-validated, wild-type ORFs, which have been previously described (*32*), represent more than 75% of annotated human kinases. The validated ORFs also include a curated collection of mutant alleles of particular relevance to melanoma and signaling molecules related to cell survival and apoptosis (fig. S6 and table S3). More than 90% of printed constructs yielded stable infection as determined by resistance to blasticidin selection, and spot-spot cross-contamination was minimal: Replicate spots containing the same ORF consistently yielded similar levels of infection, and control spots containing no virus yielded no surviving cells after selection.

Using Kinome ORF MicroSCALEs, we performed a screen to identify kinases that when overexpressed decreased the sensitivity of *B-RAF*^{V600E}–mutant melanoma cells (A375) to PLX4720, a selective inhibitor of the mitogen-activated protein kinase kinase kinase (MAPKKK) RAF (*37*–*39*). B-RAF^{V600E} exhibits constitutive activity, is a key driver mutation in melanoma, a form of skin cancer, and frequently confers sensitivity to inhibitors of the MAPK pathway (*40*) This 1-week screening assay was robust [Z' factor = 0.40 ± 0.03 (*41*)], and we maximized the dynamic range of the assay by seeding the cells at relatively low densities and halting the assay when cells became confluent (fig. S7 and Materials and Methods). Our results were in agreement with a previous screen performed with the same cell line, drug, and a largely overlapping ORF library, but performed in multiwell plate format with an independent viral preparation, different infection and assay procedures, and no blasticidin selection (Fig. 2, E and F, and table S4) (*32*). Specifically, of the 10 top-scoring wild-type ORFs from the original screen that gave efficient infection in our screen, 8 (80%) scored as hits ($P < 0.05$), 7 scored in the top 10% of all ORFs, and 5 scored in the top 4% (top 20 wild-type ORFs). These hits included genes encoding MAPKKKs *C-RAF*, *MAP3K8* (also known as *COT*), which was excluded from further analysis because of poor infection, and *MOS*, which scored weakly in the original screen (*32*). We added five MAPK pathway mutant activated alleles [*H-RAS*^{G12V}, *K-RAS*^{G12V}, *MEK1*$^{S218D/S222D}$ (*MEK*^{DD}), *MEK1*^{P124L}, and *MEK1*^{Q56P}] to the screen as positive controls. All five of these scored in the screen, including four that scored in the top 15 ORFs overall (*32*, *42*–*44*). The genes encoding platelet-derived growth factor receptor β (*PDGFR*β) and insulin-like growth factor 1 receptor (*IGF1R*), two kinases previously implicated in RAF inhibitor resistance (*45*, *46*), did not score in this or our original screen (*32*), possibly because the cells lacked sufficient amounts of ligand or accessory factors required to achieve full activation of these receptors. Finally, we used six replicate drug-treated arrays for this screen, and retrospective analysis indicated that a single array was sufficient to identify 80 ± 10% of the confirmed hits above, and three replicate arrays were sufficient to identify 90 ± 6% (fig. S8).

Systematic screens for genetic modifiers of response to targeted inhibitors

Having demonstrated that MicroSCALE screening produced data comparable to that obtained with standard multiwell plate-based screening, we designed a strategy to perform multiple functional modifier screens across related classes of drugs and combine these results with existing cell line pharmacogenomic data to nominate high-priority candidate resistance genes and pathways (Fig. 3A).

We performed functional screens in A375 cells as described above with five additional selective small-molecule inhibitors relevant to melanoma, including agents targeting RAF (GDC-0879), MEK1/2 (mitogen-activated protein kinase kinases 1 and 2) (AZD-6244 and PD-0325901), mTOR (Torin1), and both mTOR and PI3K (phosphatidylinositol 3-kinase) (BEZ-235) [fig. S9; two to five replicate arrays (screens) for each drug along with four replicate vehicle-treated arrays] (*37*, *47*–*51*). Unsupervised hierarchical clustering of both arrays and ORFs revealed several notable phenomena (Fig. 3B). First, kinome-wide modifier profiles segregated the three classes of inhibitors on the basis of their biochemical targets as expected, with replicate arrays frequently clustering together as nearest neighbors. Second, most strong hits against drugs targeting one member of the MAPK pathway (MEK1/2 or RAF) were also hits for drugs targeting the other

member. There were a few notable exceptions to this trend, including overexpression of *C-RAF* and *MOS*, which conferred selective resistance to RAF inhibitors but not MEK1/2 inhibitors. This result is expected because both C-RAF and MOS directly activate MEK (*32*, *52*). Finally, hits rarely scored for both mTOR and MAPK inhibitors, implying that genetic modifier profiles contain functional information that is specific to the

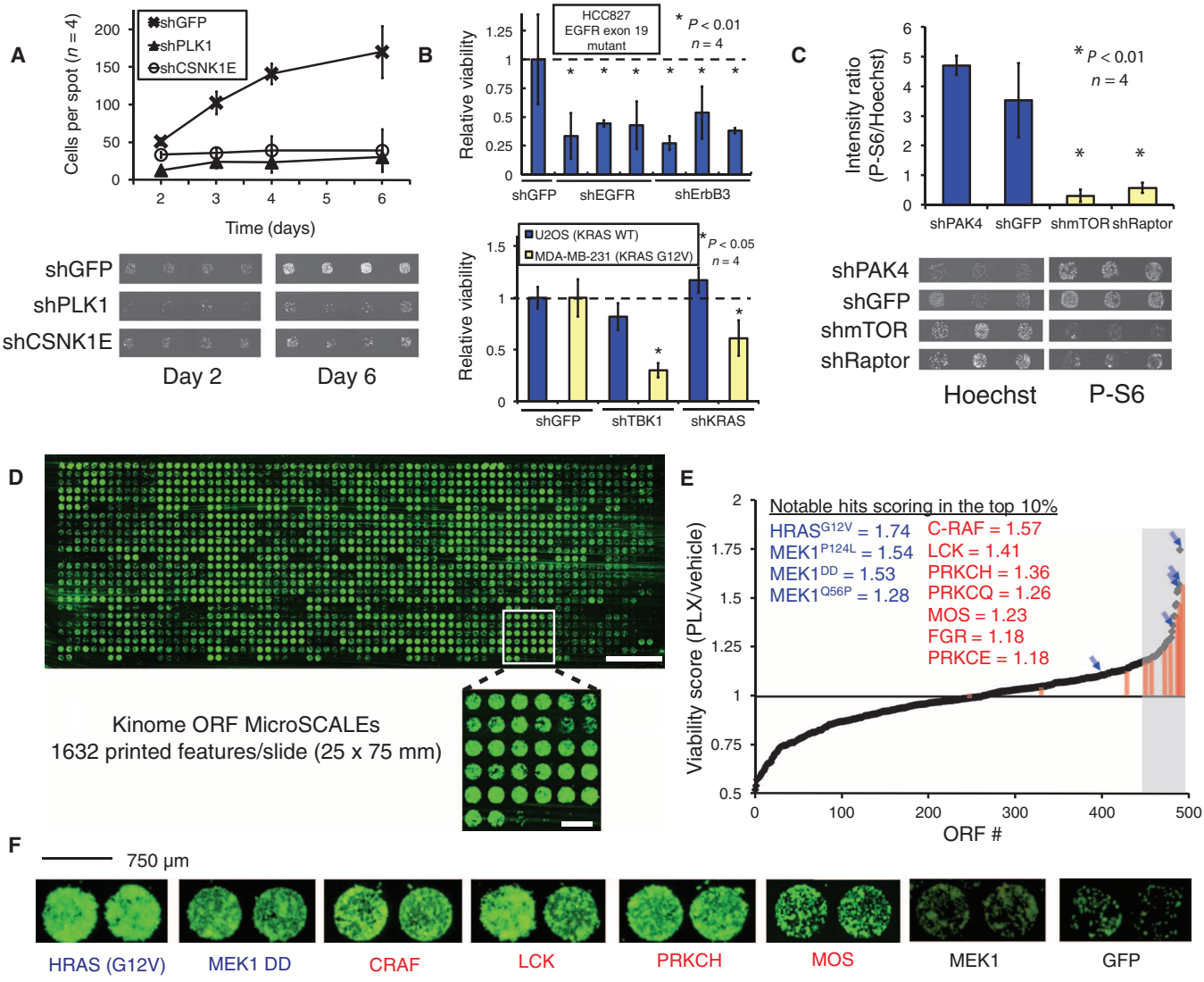

Fig. 2. MicroSCALE screening applications. (**A**) Top: Slides were fixed and stained (Hoechst) on the indicated number of days after seeding and U2OS cell numbers were determined by counting the number of nuclei per spot (n = 4 replicate spots per condition). Bottom: Images of replicate features expressing the indicated hairpins 2 and 6 days after seeding. (**B**) Slides were stained (Hoechst) on day 6 and relative viabilities were determined using the background-subtracted staining intensity on each feature (n = 4 replicate spots per condition). *P* values are relative to the shGFP control. HCC827 cells have a constitutively active mutant form of the EGFR, U2OS cells are wild type (WT) for KRAS, and MDA-MB-231 cells have a constitutively active mutant form of KRAS. (**C**) Slides were stained [Hoechst and an antibody recognizing phosphorylated S6 (P-S6)] on day 5 and total P-S6 staining intensity was background-subtracted and normalized to Hoechst intensity (n = 4 replicate spots per condition). (**D**) Kinome ORF MicroSCALE arrays. Features are 600 µm in diameter with 750-µm center-to-center spacing. The two features in the bottom right-hand corner of each 6 × 6 subgrid are control spots containing no virus. Arrays were stained (Syto82) on day 6. Scale bars, 10 mm and 1 mm (inset). (**E**) Results of a PLX4720 (1 µM) modifier screen in A375 cells. Average viability scores of individual ORFs are shown (each normalized to vehicle-only treatment), with the top 10% of ORFs shaded in gray. Red bars represent the top 10 WT ORFs from an analogous multiwell plate–based screen (*32*), and blue arrows indicate the scores of five MAPK pathway mutant positive control ORFs (see text for details; n = 12 or 18 replicate spots per ORF). The top 10% of ORFs in the screen are in the shaded region, and selected WT (red) and mutant (blue) ORFs from this region are listed along with their individual scores in the inset. (**F**) Images of replicate spots on a PLX4720-treated array, including hits from ORFs with MAPK pathway mutants (blue), hit from ORFs with WT genes (red), and ORFs with control genes (black). Cells were selected with puromycin in (A) to (C) and blasticidin in (D) to (F).

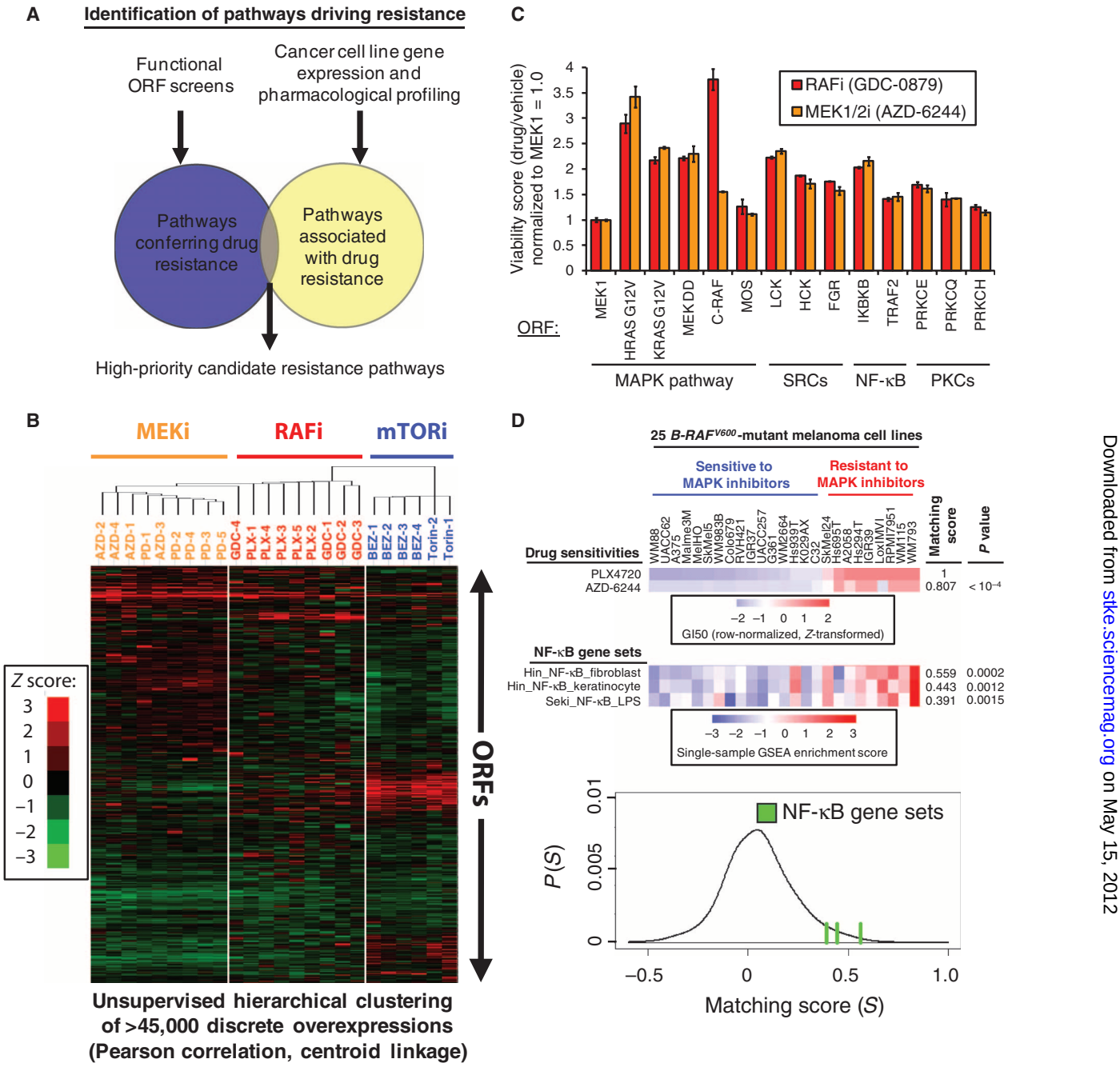

Fig. 3. Integrating the results of MicroSCALE screens with pharmacogenomic data to identify genetic modifiers of therapeutic response in melanoma. (**A**) Schematic depicting an approach to discover high-priority resistance genes and pathways. (**B**) Heat map showing the results of modifier screens. Columns represent individual arrays (two to five replicate arrays were screened for each drug), and rows represent the average proliferation score of each ORF (drug/vehicle; $n = 2$ or $n = 3$ replicate spots for each ORF on the array). Unsupervised hierarchical clustering of rows and columns was performed (for simplicity, the dendrogram representing the results of row-based clustering is not shown). Scale bar indicates Z scores (SDs from the column mean; see Materials and Methods). (**C**) Validated hits that decrease the sensitivity of A375 cells to MAPK pathway inhibitors are shown grouped into functional categories ($n = 3$ replicate wells per condition). (**D**) Top: Heat map depicting PLX4720 and AZD-6244 GI_{50} values for a panel of 25 *B-RAF*^{V600}–mutant melanoma cell lines. GI_{50} values are row (drug)–normalized and Z-transformed. Bottom: Heat map showing single-sample GSEA scores for three gene sets annotating NF-κB activation. The matching scores of the NF-κB gene sets against PLX4720's GI_{50} profile reveal a significant enrichment of those gene sets in PLX4720- and AZD-6244–resistant cell lines. [A perfect match (antimatch) corresponds to a matching score of +1(−1) and a random match to 0.] The histogram depicts the matching scores of 3264 gene sets (MSigDB/C2 v3.0) against PLX4720's GI_{50} profile, with the scores of the NF-κB gene sets highlighted by green lines.

biochemical pathway(s) perturbed by each drug. Thus, our data suggest that the overexpression of individual kinases can confer cross-resistance to multiple inhibitors targeting a single pathway, whereas individual kinases may only rarely confer cross-resistance to inhibitors targeting distinct pathways.

To validate and prioritize candidates emerging from primary screens, we selected a panel of 30 to 40 ORFs that scored in the top 15% in each individual screen with statistical significance ($P < 0.05$). We expressed each of these ORFs individually in A375 cells in a traditional multiwell plate format and measured proliferation scores (drug/vehicle) at a single drug concentration. Of the hits identified in primary screens, 74, 65, and 63% were validated as conferring at least a modest survival advantage relative to a negative control (*MEK1*) in the presence of RAF, MEK1/2, and mTOR and PI3K inhibitors, respectively (fig. S10A). In general, genes that modulate drug sensitivity segregated into defined classes and pathways (fig. S10, B and C). For example, hits modulating sensitivity to mTOR and PI3K inhibitors included protein kinase A (PKA) regulatory and catalytic subunits (*PRKAR1A*, *PRKACB*, and *PRKACG*) and established PI3K-mTOR pathway–associated genes (*RPS6KA5*, encoding ribosomal protein S6 kinase α5; *PIK3CG*, encoding PI3Kγ; and *PIP5K3*, encoding 1-phosphatidylinositol-3-phosphate 5-kinase), whereas those modulating sensitivity to both RAF and MEK1/2 inhibitors included multiple SRC-family kinases (*LCK*, encoding lymphocyte-specific protein tyrosine kinase; *HCK*, encoding hemopoietic cell kinase; and *FGR*, encoding the Gardner-Rasheed feline sarcoma viral oncogene homolog) and the novel protein kinase C (PKC) isozymes (*PRKCE*, *PRKCQ*, and *PRKCH*). We also found that several nuclear factor κB (NF-κB) pathway members scored in primary screens against RAF and MEK1/2 inhibitors. We validated two of these genes, *IKBKB*, encoding IκB (inhibitor of NF-κB) kinase β, a subunit of the IκB kinase complex, and *TRAF2*, encoding tumor necrosis factor (TNF) receptor–associated factor 2, in secondary assays (Fig. 3C).

Integrating functional screens with large-scale pharmacogenomic data

Existing pharmacogenomic data sets provide an independent means of identifying genes and pathways associated with resistance that can be used to complement and prioritize the findings emerging from large-scale functional screens. Using a panel of 25 *B-RAF*^{V600}–mutant melanoma cell lines for which steady-state gene expression (mRNA) and pharmacological sensitivity data are available (see Materials and Methods) (*32*), we first identified cell lines that were sensitive or resistant to RAF and MEK1/2 inhibitors (fig. S11). To determine whether resistant cell lines shared common transcriptional signatures, we performed single-sample Gene Set Enrichment Analysis (GSEA) (*4*, *53*) to identify gene sets whose pattern of expression across the entire panel of cell lines most strongly correlated with the observed pattern of MAPK inhibitor resistance. Notably, we found a significant enrichment of multiple independent gene sets associated with NF-κB pathway activation in resistant cell lines compared with sensitive lines (Fig. 3D), consistent with the results of our large-scale functional screens, which found that the overexpression of NF-κB pathway genes conferred selective resistance to MAPK inhibitors (Fig. 3C and fig. S12).

Validation of NF-κB pathway members as mediators of resistance to MAPK pathway inhibitors

The identification of the NF-κB pathway through two independent, orthogonal approaches suggested that this pathway may be capable of modulating the sensitivity of melanomas to MAPK pathway inhibitors. To functionally validate this finding, we measured the effect of NF-κB activation on the half-maximal growth inhibitory concentrations (GI_{50}s) of PLX4720, AZD-6244, and Vertex 11e, a selective ERK2 (extracellular signal–regulated kinase 2) inhibitor (*54*), in four *B-RAF*^{V600}–mutant melanoma cell lines (A375, Colo679, UACC62, and SkMel28). Overexpression of *IKBKB* or *TRAF2* (Fig. 4A) conferred 1.5- to 10-fold GI_{50} shifts relative to *MEK1* overexpression, which had no effect on GI_{50} relative to uninfected parental cells and was therefore used as a negative control (fig. S13). Drug resistance could also be induced in all cell lines by the addition of soluble TNFα, an established NF-κB agonist (Fig. 4A) (*55*). In A375 and UACC62 cells, the magnitude of the PLX4720 GI_{50} shift conferred by *IKBKB* or *TRAF2* overexpression or TNFα addition was comparable to that observed with *C-RAF* overexpression, a well-established mediator of resistance to RAF inhibitors (fig. S13) (*52*). Immunoblot analysis indicated that in A375 (Fig. 4B) and SkMel28 cells (fig. S14), overexpression of *IKBKB* or *TRAF2* or exogenous TNFα, in the presence or absence of PLX4720, stimulated RelA phosphorylation [a commonly used measure of NF-κB pathway activity (*55*)] to varying amounts but failed to promote ERK phosphorylation in the presence of PLX4720. In A375 cells (Fig. 4C) and Colo679 cells (fig. S15), NF-κB stimulation was also associated with resistance to PLX4720-induced apoptosis but did not bypass drug-induced cell cycle arrest.

Finally, our findings raised the possibility that NF-κB activity might predict clinical responses to MAPK inhibitors. As an initial test of this hypothesis, we used human-derived *B-RAF*^{V600} malignant melanoma short-term cultures. We first queried steady-state gene expression data from 29 cultures for signatures of NF-κB pathway activity (*56*). We selected four cultures that we predicted, on the basis of high NF-κB activity, to be resistant to MAPK inhibitors and four that we predicted, on the basis of low NF-κB activity, to be sensitive to MAPK inhibitors. Strikingly, all four high NF-κB cultures were strongly resistant to all MAPK pathway inhibitors with the exception of WM1930, which was partially sensitive to AZD-6244. Conversely, all four cultures with low NF-κB activity were sensitive to MAPK inhibitors as expected (Fig. 4D; matching score = 0.906, $P = 0.0086$). Together, these data provide evidence that NF-κB pathway activity may predict clinical efficacy of MAPK inhibitors and play a functional role in the responses of human patients to these drugs.

DISCUSSION

Our results demonstrate the design, scalability, and screening applications of MicroSCALE, a high-throughput platform that overcomes the major limitations that have historically prevented the deployment of cell microarrays in functional genomics. Cell and reagent requirements for MicroSCALE screens are about 10- to 25-fold lower than those for analogous 384-well plate-based screens, and we estimate that throughput and costs may be similarly improved, although the latter estimates may vary across different screening libraries, formats, and centers (table S5). Further, MicroSCALE screens can be performed in any standard biological laboratory without requiring specialized facilities. Given these advantages, we anticipate that this technology may broaden the scope of functional genomic screens, particularly those that require large combinations of cell lines, perturbations, and assay outputs or those involving cell-, reagent-, or resource-limited settings. Potential settings in which this technology may not be useful may include screens involving phenotypes with low penetrance that require large numbers of cells per perturbation; screens involving nonadherent cells; and screens that require physical isolation of the medium associated with each perturbation, such as those involving secreted factors.

Drug modifier screens are one useful application of MicroSCALE because they have the potential to systematically reveal the genes and pathways that modulate drug sensitivity (*32*, *57*, *58*). To date, large-scale genetic modifier screens in mammalian cells have been limited in part

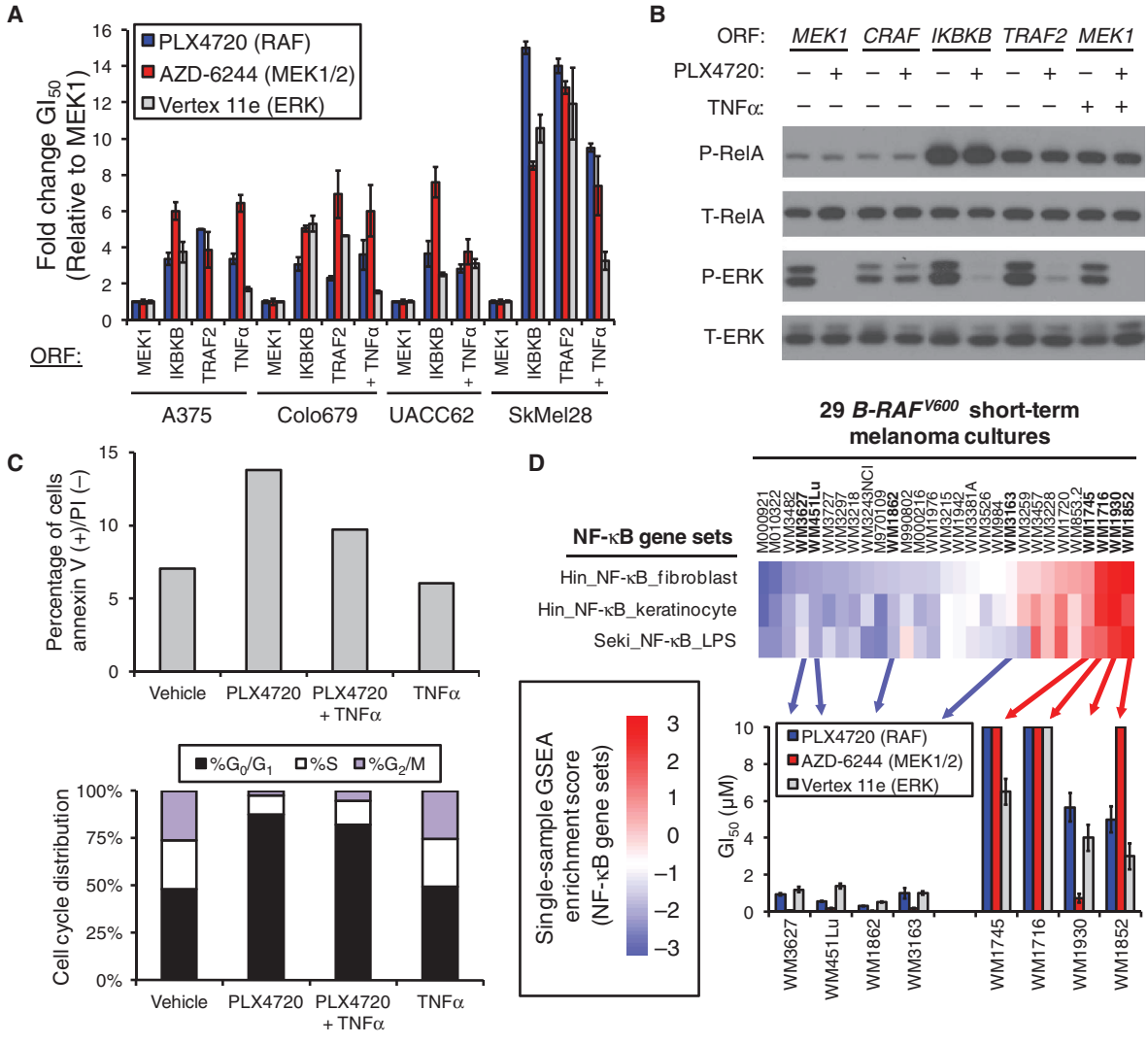

Fig. 4. Effects of NF-κB activation in *B-RAF*^{V600}–mutant melanomas treated with MAPK pathway inhibitors. (**A**) Effects of *IKBKB* or *TRAF2* overexpression or the addition of exogenous TNFα (25 ng/ml) on GI_{50} concentrations for RAF, MEK1/2, or ERK2 inhibitors in four *B-RAF*^{V600}–mutant melanoma cell lines (n = 3 replicate GI_{50} curves per condition). Overexpression of *MEK1* serves as a negative control. (**B**) Effects of *IKBKB* or *TRAF2* overexpression or exogenous TNFα (25 ng/ml) on phosphorylation of RelA and phosphorylation of ERK in the presence of PLX4720 (A375 cells; three replicate experiments were performed and representative blots are shown). MEK1 serves as a negative control ORF. C-RAF serves as a positive control ORF that activates the MAPK pathway in the presence of PLX4720. (**C**) Effects of exogenous TNFα (25 ng/ml) on apoptosis induction [as indicated by annexin V (+)/PI (–) staining] and cell cycle arrest induced by PLX4720 (A375 cells; three replicate experiments were performed and representative plots are shown). (**D**) Correlation between NF-κB gene expression signatures and resistance to MAPK pathway inhibitors in patient-derived *B-RAF*^{V600}–mutant melanoma short-term cultures (n = 3 replicate GI_{50} curves per condition). Cell lines with corresponding GI_{50} data are in bold. The y axis does not extend beyond 10 μM, which is the upper limit of this assay.

by the practical limitations associated with screening across many drugs or cell lines by means of existing screening technologies. We performed 45,000 discrete ORF overexpression and drug treatment measurements, a scale that would be difficult and costly to achieve with existing technologies (table S5), to generate kinome-wide drug modifier profiles across multiple classes of inhibitors. This analysis revealed several new insights. First, modifier screens reliably uncovered genes and pathways whose activation conferred drug resistance in a target- and pathway-selective manner, including some that are known to be clinically relevant (for example, *C-RAF*, genes encoding SRC kinases, and *COT*) (*32*, *52*, *59*). Second, our evidence suggests that drugs targeting common biochemical nodes or pathways will exhibit highly similar modifier profiles, reflecting their shared mechanisms of action, whereas those targeting distinct pathways will exhibit unique profiles, reflecting distinct mechanisms of action. This finding suggests that, when performed in sufficient scale, such as with many compounds, ORF-based modifier screens may ultimately be used to functionally annotate heretofore uncharacterized small-molecule probes emerging from drug discovery pipelines (*36*, *37*). Third, our observation

that inhibitors of the MAPK, mTOR, and PI3K signaling pathways have almost entirely nonoverlapping modifier profiles suggests that the spectrum of events that can confer cross-resistance to inhibitors of independent signaling pathways may be considerably narrower than the spectrum of events that can confer cross-resistance to multiple compounds targeting the same pathway. This observation provides empirical support for the idea of testing combination therapies that inhibit independent signaling pathways as a means of preventing the emergence of drug resistance.

Finally, by integrating our large-scale functional screening data with steady-state gene expression and pharmacological sensitivity profiling, we nominated NF-κB pathway components as mediators of resistance to MAPK pathway inhibitors. These data are consistent with the finding that TNFα can block apoptosis induced by MEK1/2 inhibitors (*60*), a report demonstrating that NF-κB may mediate resistance to EGFR inhibitors in *EGFR*-mutant lung cancers (*61*), and the established links between NF-κB activity and resistance to chemotherapy and ionizing radiation (*62*). These findings may inform upcoming clinical trials for melanoma and other cancers that use targeted and immunotherapy drug combinations that impinge on both MAPK and NF-κB signaling (*63*–*66*). Overall, the widespread deployment of the approaches described here holds considerable potential for the scalable interrogation of many phenotypes linked to human biology and disease.

MATERIALS AND METHODS

Cell lines and reagents

A375, Colo679, UACC62, Malme3M, WM793, WM1716, WM1745, WM1852, WM1930, SkBr3, HCC827, UACC812, ZR75-1, WM3627, WM451Lu, WM1862, and WM3163 were grown in RPMI with 10% fetal bovine serum (FBS) and 1% penicillin/streptomycin. SkMel28, SkMel5, Lox IMVI, IGR39, Hs294T, A2058, A549, U2OS, U87, SW620, HBL100, MCF7, PC3, MDA-MB-231, MDA-MB-453, SW480, HCT116, DDLS8817, LPS141, and $p53^{-/-}$ mouse embryonic fibroblasts were grown in Dulbecco's modified Eagle's medium (DMEM) with 10% FBS and 1% penicillin/streptomycin. HeLa, 786-0, HepG2, DU145, 90-8T, 293T, and Panc1 were grown in DMEM with 10% heat-inactivated FBS and 1% penicillin/streptomycin. WM115 and RPMI7951 were grown in MEM (minimum essential media) with 10% FBS and 1% penicillin/streptomycin. Human mammary epithelial cell derivatives were grown in serum-free MEGM (mammary epithelial cell growth medium) as previously described (*67*). PLX4720, GDC-0879, AZD-6244, PD-0325901, and BEZ-235 were purchased from Selleck Chemicals. Torin1 was obtained from N. S. Gray (Dana-Farber Cancer Institute). Compound 11e was a gift from Vertex Pharmaceuticals.

Immunoblots and immunofluorescence

Immunoblotting was performed as previously described (*32*) and blots were probed with primary antibodies recognizing phospho-RelA (Ser^{536}, 1:1000, Cell Signaling), RelA (1:1000, Cell Signaling), phospho-ERK1/2 (Thr^{202}/Tyr^{204}, 1:1000, Cell Signaling), and ERK1/2 (1:1000, Cell Signaling). Immunofluorescence was performed by fixing slides with 3.7% paraformaldehyde, permeabilizing with 0.1% Triton X-100, and staining at indicated dilutions in 1% bovine serum albumin. Immunofluorescence stains were Hoechst (1:10,000, Invitrogen), Syto82 (1:5000, Invitrogen), Alexa Fluor 546–phalloidin (1:1000, Invitrogen), phospho-S6 ($Ser^{235/236}$, 1:1000, Cell Signaling), and p24 (1:500, ZeptoMetrix).

Image acquisition and analysis

Images in Figs. 1 and 2, A to C, and figs. S1, S2, S4, and S6 were acquired with an Axiovert 200 microscope (Carl Zeiss) and analyzed with National Institutes of Health ImageJ software. Images of Syto82-stained arrays and associated data in Figs. 2, D to F, and 3 and fig. S5 were obtained with an Axon GenePix 4000B microarray scanner, and spot intensities were analyzed with GenePix analysis software.

Production of MicroSCALE slides

Lentiviruses expressing shRNAs or full-length ORFs were produced and titered in high-throughput 96-well format as previously described (*3*, *6*, *32*). Stock solutions of polybrene (Sigma) and chondroitin sulfate (Sigma) were dissolved at 8 mg/ml in phosphate-buffered saline and sterile-filtered. The two solutions were sequentially added to 1 ml of each lentiviral supernatant (in deep, v-bottom 96-well plates) to yield a final concentration of each polymer of 400 μg/ml. Solutions were then incubated for 15 min at room temperature. Plates were next centrifuged at 1150*g* for 20 min, after which supernatants were aspirated with a multichannel wand aspirator. Thirty microliters of lentivirus printing buffer [containing 0.4 M Hepes, 1.23 M KCl, trehalose (12.5 mg/ml), and protamine sulfate (12 μg/ml), pH adjusted to 7.3] was added to each well, and lentiviral pellets were mechanically resuspended and transferred to 384-well, round-bottom source plates for printing. All fluid handling was performed with a Janus automated liquid handling workstation. MicroSCALE slides were printed by use of a two-stage process onto polyacrylamide hydrogel–coated glass slides (CodeLink, SurModics) with an Aushon 2470 microarray printer. First, gelatin (type B, bovine, Sigma) was dissolved at 2 mg/ml in deionized water containing 0.1% glycerol and printed to yield cell adhesive islands; then, individual, concentrated lentivirus preparations were printed directly on top of gelatin features. During the technological development phase of this work, solid pins of multiple sizes were used, resulting in feature sizes ranging from 200 to 500 μm in diameter (spot sizes are indicated in each figure). Kinome ORF MicroSCALEs were printed with a pin that yields features that are about 600 μm in diameter with 750-μm center-center spacing. Larger pins were chosen for these arrays to maximize the signal and dynamic range of drug modifier assays. After printing, slides were stored in vacuum-sealed bags at −80°C until ready to use.

MicroSCALE functional assays and high-throughput screens

Slides were thawed at room temperature, blocked for 30 min with DMEM + 10% FBS, and seeded with 1×10^5 to 5×10^5 cells per slide in four-well slide chambers. Cells were allowed to attach and become infected on MicroSCALE features overnight and were then selected with puromycin (2.5 μg/ml) or blasticidin (10 μg/ml). For assays described in Figs. 1 and 2, A to C, figs. S1, S2, S4, and S6, and tables S1 and S2, cells were incubated, fixed, stained, and imaged as indicated in the figure legends. For high-throughput ORF modifier screens, cells were selected for 2 days with blasticidin and then incubated for 5 to 7 days in normal growth medium containing blasticidin and the indicated drugs: PLX4720 (1 μM), GDC-0879 (1 μM), AZD-6244 (250 nM), PD-0325901 (250 nM), BEZ-235 (200 nM), Torin1 (200 nM), or vehicle [dimethyl sulfoxide (DMSO)]. Slides were then stained with Syto82 and imaged as described above.

Analysis of screening data

Raw values corresponding to Syto82 fluorescence intensity on each MicroSCALE feature were first normalized by applying a local median smoothening algorithm that calculated the difference between the raw intensity of each feature and the median intensity of its six nearest neighbors in each *x*-*y* direction. This approach, commonly used in the analysis of DNA or protein microarrays, adjusts for variations in cell density or autofluorescence across the slide surface (*68*). Individual feature values were then normalized to the median value on the slide and then to the average normalized value of the same feature on four replicate, vehicle-treated slides

(viability score). Finally, individual spot viability scores were *Z*-transformed to indicate their distance (in number of SDs) from the array mean, and the average value for two to three replicate spots per ORF was calculated (*41*). Hierarchical clustering of these data was performed with Cluster 3.0 and visualized with Java TreeView.

Secondary growth-inhibition assays

ORF-expressing lentiviruses used in secondary assays were produced as previously described (*32*). Cells were infected at a 1:10 to 1:20 dilution of virus in six-well plates in the presence of polybrene (7.5 μg/ml) and centrifuged at 1200*g* for 1 hour at 37°C. Twenty-four hours after infection, blasticidin (10 μg/ml) was added and cells were selected for 48 hours. Cells were then trypsinized, counted, and seeded into 96-well plates at 2000 cells per well for growth-inhibition assays. Twenty-four hours later, DMSO or concentrated serial dilutions of indicated drugs (in DMSO) were added to cells (1:1000) to yield final drug concentrations of 100, 10, 1, 0.1, 0.01, 0.001, 0.0001, or 0.00001 μM. Cell viability was measured 4 days after drug addition with CellTiter-Glo luminescent viability assay (Promega). Viability was calculated as the percentage of control (untreated cells) after background subtraction. A minimum of six replicates were performed for each cell line/ORF/drug/concentration. Data from growth-inhibition assays were displayed with GraphPad Prism 5 for Windows (GraphPad). GI_{50} values were determined as the drug dose corresponding to half-maximal growth inhibition as previously described (*32*). Growth curves that crossed the 50% inhibition point at or above 10 μM have GI_{50} values annotated simply as >10 μM. GI_{50} values for unmodified parental cells were determined by seeding cells directly into 96-well plates and conducting assays as described above. For single-dose studies, cells were seeded at 500 cells per well in 96-well plates, infected at 24 hours with a 1:20 dilution of virus in the presence of polybrene (7.5 μg/ml) followed by centrifugation at 1200*g* for 1 hour at 37°C, selected with blasticidin (10 μg/ml) for 48 hours, and then treated with drug or vehicle and assayed for viability with CellTiter-Glo as above after a 4-day incubation. Viability was calculated as the percentage of control (vehicle-treated cells) after background subtraction.

Analysis of cell cycle and apoptosis

Cells were seeded into 10-cm dishes on day 0; treated as indicated with PLX4720 (1 μM), TNFα (25 ng/ml), or vehicle on day 1; and analyzed on day 3. For the analysis of cell cycle distributions, cells were fixed with 80% ethanol in water and stained with propidium iodide (PI) (50 μg/ml; BD Pharmingen) containing ribonuclease A (0.1 mg/ml) and 0.05% Triton X-100. For the analysis of annexin V staining, cells were suspended in annexin V binding buffer (10 mM Hepes, 140 mM NaCl, and 2.5 mM $CaCl_2$, pH 7.4) containing annexin V–APC (allophycocyanin) (BD Pharmingen) and PI (50 μg/ml). For both analyses, a minimum of 50,000 events were counted per sample. Cell cycle data were analyzed with ModFit software. Annexin V staining was analyzed with FlowJo software, with annexin V–positive cells defined as those exhibiting annexin V staining intensities exceeding 99.9% of cells in a PI-only control sample.

Cancer Cell Line Encyclopedia data

Gene expression and pharmacological sensitivity data for 25 *B-RAF*^{V600}–mutant melanoma cell lines were obtained by the Cancer Cell Line Encyclopedia (CCLE) project, a collaboration between the Broad Institute, the Novartis Institutes for Biomedical Research, and the Genomics Institute of the Novartis Research Foundation. RMA (robust multichip average)–normalized mRNA expression data were collapsed according to per-sample maximum probe values with the collapse data set function of GSEA desktop (http://www.broadinstitute.org/gsea/index.jsp).

Gene expression analysis

The single-sample GSEA enrichment scores used in Figs. 3D and 4D were obtained as described by Barbie *et al*. (*4*). Briefly, for every gene expression sample profile, the values were first rank-normalized and sorted and then a single-sample enrichment score for each gene set was computed on the basis of the integrated difference between the empirical cumulative distribution functions of the genes in the gene set versus the rest. This procedure is similar to the computation of standard GSEA (*53*) but is based on absolute rather than differential expression. Published details of this method and other applications are available (*53*, *69*, *70*). The full names of gene sets referenced in the text and figures are hinata_nfkb_targets_fibroblast_up ("Hin_NF-κB_fibroblast"), hinata_nfkb_targets_keratinocyte_up ("Hin_NF-κB_keratinocyte"), and seki_inflammatory_response_lps_up ("Seki_NF-κB_LPS"). Matching scores between PLX4720 versus single-sample GSEA gene set scores (Fig. 3D) were obtained by a normalized and rescaled mutual information estimate. Briefly, we consider the differential mutual information (*71*) between two continuous vectors x (target, for example, PLX4720 resistance) and y (feature, for example, an NF-κB gene set): $I(x, y) = \iint P(x, y) \log_2(P(x, y)/(P(x)P(y)))dxdy$ and estimate this quantity with a kernel-density estimate of the joint distribution $\hat{P}(x,y)$. The discrete data are smoothed with a Gaussian kernel, with width determined by a cross-validation bandwidth estimation (*72*) at each data point (x_i, y_i), and $\hat{P}(x,y)$ is found by summing overall densities over a discrete grid (100 × 100). The resulting estimate of differential mutual information, $\hat{I}(x,y)$, is then normalized (*73*, *74*) by the joint entropy $\hat{H}(x,y) = \iint \hat{P}(x,y)\log_2\hat{P}(x,y)dxdy$, to obtain $U(x,y) = \hat{I}(x,y)/\hat{H}(x,y)$. Finally, the matching score is obtained by rescaling $U(x, y)$ using the normalized mutual information of x (the target) with itself and adding a "direction" (±) according to the Pearson correlation $\rho(x, y)$: $S(x, y) = \text{sign}(\rho(x, y))U(x, y)/U(x, x)$. A perfect match (antimatch) corresponds to a score of +1(−1) and a random match to 0. The significance of a given match $S(x, y)$ is estimated by a permutation test where the values of x are randomly permutated 10,000 times, and a nominal P value is computed according to how many times the matching scores of the random permutations are higher than the actual score. This matching score $S(x, y)$ has advantages over other metrics including increased sensitivity to nonlinear associations and wider dynamic range at the top of the matching scale.

Statistics

Results are expressed as the means ± SD. For comparisons between two groups, P values were calculated with unpaired, two-tailed Student's t tests.

SUPPLEMENTARY MATERIALS

www.sciencesignaling.org/cgi/content/full/5/224/rs4/DC1

Fig. S1. Strategy for restricting cell adhesion to printed features.
Fig. S2. Requirement for purification and concentration of lentiviruses before microarray printing.
Fig. S3. High-throughput lentivirus concentration using polyelectrolyte complexation.
Fig. S4. Puromycin selection of infected cells on MicroSCALE features.
Fig. S5. Quantification of cell number on MicroSCALE features using a DNA microarray scanner.
Fig. S6. Printing and infections with ORF-expressing lentiviruses containing inserts of varying sizes.
Fig. S7. Modifier screening pipeline.
Fig. S8. Percentage of the total validated hits identified in a screen with six replicate arrays as a function of the number of replicate (drug-treated) microarrays used.
Fig. S9. Sensitivity of A375 and MDA-MB-453 cells to targeted inhibitors.
Fig. S10. Confirmation of hits identified in primary screens.
Fig. S11. GI_{50} concentrations for *B-RAF*^{V600}–mutant melanoma cell lines treated with MAPK inhibitors.
Fig. S12. Effect of *IKBKB* overexpression on sensitivity to inhibitors of the MAPK pathway and the mTOR and PI3K pathway.

Fig. S13. Comparison of resistance to PLX4720 conferred by overexpression of *IKBKB*, exogenous TNFα, or overexpression of *C-RAF*.
Fig. S14. Phosphorylation of RelA and ERK in response to NF-κB pathway manipulations and PLX4720 treatment in SkMel28 cells.
Fig. S15. Effects of TNFα on PLX4720-induced apoptosis and cell cycle arrest in Colo679 cells.
Table S1. Examples of cell lines compatible with MicroSCALE screening.
Table S2. Examples of cell lines incompatible with MicroSCALE screening.
Table S3. Constructs present on Kinome ORF MicroSCALEs.
Table S4. Results of a PLX4720 modifier screen in A375 cells. (Excel file)
Table S5. Materials requirements and throughput estimates for kinome-scale drug modifier screens in MicroSCALE and 384-well formats.

REFERENCES AND NOTES

1. S. D. Shapira, I. Gat-Viks, B. O. Shum, A. Dricot, M. M. de Grace, L. Wu, P. B. Gupta, T. Hao, S. J. Silver, D. E. Root, D. E. Hill, A. Regev, N. Hacohen, A physical and regulatory map of host-influenza interactions reveals pathways in H1N1 infection. *Cell* **139**, 1255–1267 (2009).
2. A. L. Brass, D. M. Dykxhoorn, Y. Benita, N. Yan, A. Engelman, R. J. Xavier, J. Lieberman, S. J. Elledge, Identification of host proteins required for HIV infection through a functional genomic screen. *Science* **319**, 921–926 (2008).
3. J. Moffat, D. A. Grueneberg, X. Yang, S. Y. Kim, A. M. Kloepfer, G. Hinkle, B. Piqani, T. M. Eisenhaure, B. Luo, J. K. Grenier, A. E. Carpenter, S. Y. Foo, S. A. Stewart, B. R. Stockwell, N. Hacohen, W. C. Hahn, E. S. Lander, D. M. Sabatini, D. E. Root, A lentiviral RNAi library for human and mouse genes applied to an arrayed viral high-content screen. *Cell* **124**, 1283–1298 (2006).
4. D. A. Barbie, P. Tamayo, J. S. Boehm, S. Y. Kim, S. E. Moody, I. F. Dunn, A. C. Schinzel, P. Sandy, E. Meylan, C. Scholl, S. Frohling, E. M. Chan, M. L. Sos, K. Michel, C. Mermel, S. J. Silver, B. A. Weir, J. H. Reiling, Q. Sheng, P. B. Gupta, R. C. Wadlow, H. Le, S. Hoersch, B. S. Wittner, S. Ramaswamy, D. M. Livingston, D. M. Sabatini, M. Meyerson, R. K. Thomas, E. S. Lander, J. P. Mesirov, D. E. Root, D. G. Gilliland, T. Jacks, W. C. Hahn, Systematic RNA interference reveals that oncogenic *KRAS*-driven cancers require TBK1. *Nature* **462**, 108–112 (2009).
5. S. Mohr, C. Bakal, N. Perrimon, Genomic screening with RNAi: Results and challenges. *Annu. Rev. Biochem.* **79**, 37–64 (2010).
6. D. E. Root, N. Hacohen, W. C. Hahn, E. S. Lander, D. M. Sabatini, Genome-scale loss-of-function screening with a lentiviral RNAi library. *Nat. Methods* **3**, 715–719 (2006).
7. M. R. Schlabach, J. Luo, N. L. Solimini, G. Hu, Q. Xu, M. Z. Li, Z. Zhao, A. Smogorzewska, M. E. Sowa, X. L. Ang, T. F. Westbrook, A. C. Liang, K. Chang, J. A. Hackett, J. W. Harper, G. J. Hannon, S. J. Elledge, Cancer proliferation gene discovery through functional genomics. *Science* **319**, 620–624 (2008).
8. J. M. Silva, K. Marran, J. S. Parker, J. Silva, M. Golding, M. R. Schlabach, S. J. Elledge, G. J. Hannon, K. Chang, Profiling essential genes in human mammary cells by multiplex RNAi screening. *Science* **319**, 617–620 (2008).
9. B. Luo, H. W. Cheung, A. Subramanian, T. Sharifnia, M. Okamoto, X. Yang, G. Hinkle, J. S. Boehm, R. Beroukhim, B. A. Weir, C. Mermel, D. A. Barbie, T. Awad, X. Zhou, T. Nguyen, B. Piqani, C. Li, T. R. Golub, M. Meyerson, N. Hacohen, W. C. Hahn, E. S. Lander, D. M. Sabatini, D. E. Root, Highly parallel identification of essential genes in cancer cells. *Proc. Natl. Acad. Sci. U.S.A.* **105**, 20380–20385 (2008).
10. K. Berns, E. M. Hijmans, J. Mullenders, T. R. Brummelkamp, A. Velds, M. Heimerikx, R. M. Kerkhoven, M. Madiredjo, W. Nijkamp, B. Weigelt, R. Agami, W. Ge, G. Cavet, P. S. Linsley, R. L. Beijersbergen, R. Bernards, A large-scale RNAi screen in human cells identifies new components of the p53 pathway. *Nature* **428**, 431–437 (2004).
11. J. S. Boehm, W. C. Hahn, Towards systematic functional characterization of cancer genomes. *Nat. Rev. Genet.* **12**, 487–498 (2011).
12. S. R. Collins, J. S. Weissman, N. J. Krogan, From information to knowledge: New technologies for defining gene function. *Nat. Methods* **6**, 721–723 (2009).
13. D. B. Wheeler, A. E. Carpenter, D. M. Sabatini, Cell microarrays and RNA interference chip away at gene function. *Nat. Genet.* **37** (suppl.), S25–S30 (2005).
14. M. L. Yarmush, K. R. King, Living-cell microarrays. *Annu. Rev. Biomed. Eng.* **11**, 235–257 (2009).
15. J. Ziauddin, D. M. Sabatini, Microarrays of cells expressing defined cDNAs. *Nature* **411**, 107–110 (2001).
16. S. Mousses, N. J. Caplen, R. Cornelison, D. Weaver, M. Basik, S. Hautaniemi, A. G. Elkahloun, R. A. Lotufo, A. Choudary, E. R. Dougherty, E. Suh, O. Kallioniemi, RNAi microarray analysis in cultured mammalian cells. *Genome Res.* **13**, 2341–2347 (2003).
17. J. M. Silva, H. Mizuno, A. Brady, R. Lucito, G. J. Hannon, RNA interference microarrays: High-throughput loss-of-function genetics in mammalian cells. *Proc. Natl. Acad. Sci. U.S.A.* **101**, 6548–6552 (2004).
18. J. K. Rantala, R. Makela, A. R. Aaltola, P. Laasola, J. P. Mpindi, M. Nees, P. Saviranta, O. Kallioniemi, A cell spot microarray method for production of high density siRNA transfection microarrays. *BMC Genomics* **12**, 162 (2011).
19. H. J. Warnatz, R. Querfurth, A. Guerasimova, X. Cheng, S. A. Haas, A. L. Hufton, T. Manke, D. Vanhecke, W. Nietfeld, M. Vingron, M. Janitz, H. Lehrach, M. L. Yaspo, Functional analysis and identification of *cis*-regulatory elements of human chromosome 21 gene promoters. *Nucleic Acids Res.* **38**, 6112–6123 (2010).
20. S. Rajan, H. Djambazian, H. C. P. Dang, R. Sladek, T. J. Hudson, The living microarray: A high-throughput platform for measuring transcription dynamics in single cells. *BMC Genomics* **12**, 115 (2011).
21. H. E. Grecco, P. Roda-Navarro, A. Girod, J. Hou, T. Frahm, D. C. Truxius, R. Pepperkok, A. Squire, P. I. H. Bastiaens, In situ analysis of tyrosine phosphorylation networks by FLIM on cell arrays. *Nat. Methods* **7**, 467–472 (2010).
22. C. Doil, N. Mailand, S. Bekker-Jensen, P. Menard, D. H. Larsen, R. Pepperkok, J. Ellenberg, S. Panier, D. Durocher, J. Bartek, J. Lukas, C. Lukas, RNF168 binds and amplifies ubiquitin conjugates on damaged chromosomes to allow accumulation of repair proteins. *Cell* **136**, 435–446 (2009).
23. B. Neumann, T. Walter, J. K. Heriche, J. Bulkescher, H. Erfle, C. Conrad, P. Rogers, I. Poser, M. Held, U. Liebel, C. Cetin, F. Sieckmann, G. Pau, R. Kabbe, A. Wunsche, V. Satagopam, M. H. A. Schmitz, C. Chapuis, D. W. Gerlich, R. Schneider, R. Eils, W. Huber, J. M. Peters, A. A. Hyman, R. Durbin, R. Pepperkok, J. Ellenberg, Phenotypic profiling of the human genome by time-lapse microscopy reveals cell division genes. *Nature* **464**, 721–727 (2010).
24. S. N. Bailey, S. M. Ali, A. E. Carpenter, C. O. Higgins, D. M. Sabatini, Microarrays of lentiviruses for gene function screens in immortalized and primary cells. *Nat. Methods* **3**, 117–122 (2006).
25. B. Neumann, M. Held, U. Liebel, H. Erfle, P. Rogers, R. Pepperkok, J. Ellenberg, High-throughput RNAi screening by time-lapse imaging of live human cells. *Nat. Methods* **3**, 385–390 (2006).
26. C. Conrad, H. Erfle, P. Warnat, N. Daigle, T. Lörch, J. Ellenberg, R. Pepperkok, R. Eils, Automatic identification of subcellular phenotypes on human cell arrays. *Genome Res.* **14**, 1130–1136 (2004).
27. X. Yang, J. S. Boehm, X. Yang, K. Salehi-Ashtiani, T. Hao, Y. Shen, R. Lubonja, S. R. Thomas, O. Alkan, T. Bhimdi, T. M. Green, C. M. Johannessen, S. J. Silver, C. Nguyen, R. R. Murray, H. Hieronymus, D. Balcha, C. Fan, C. Lin, L. Ghamsari, M. Vidal, W. C. Hahn, D. E. Hill, D. E. Root, A public genome-scale lentiviral expression library of human ORFs. *Nat. Methods* **8**, 659–661 (2011).
28. C. J. Flaim, S. Chien, S. N. Bhatia, An extracellular matrix microarray for probing cellular differentiation. *Nat. Methods* **2**, 119–125 (2005).
29. D. G. Anderson, S. Levenberg, R. Langer, Nanoliter-scale synthesis of arrayed biomaterials and application to human embryonic stem cells. *Nat. Biotechnol.* **22**, 863–866 (2004).
30. J. Reiser, Production and concentration of pseudotyped HIV-1-based gene transfer vectors. *Gene Ther.* **7**, 910–913 (2000).
31. J. M. Le Doux, N. Landazuri, M. L. Yarmush, J. R. Morgan, Complexation of retrovirus with cationic and anionic polymers increases the efficiency of gene transfer. *Hum. Gene Ther.* **12**, 1611–1621 (2001).
32. C. M. Johannessen, J. S. Boehm, S. Y. Kim, S. R. Thomas, L. Wardwell, L. A. Johnson, C. M. Emery, N. Stransky, A. P. Cogdill, J. Barretina, G. Caponigro, H. Hieronymus, R. R. Murray, K. Salehi-Ashtiani, D. E. Hill, M. Vidal, J. J. Zhao, X. Yang, O. Alkan, S. Kim, J. L. Harris, C. J. Wilson, V. E. Myer, P. M. Finan, D. E. Root, T. M. Roberts, T. Golub, K. T. Flaherty, R. Dummer, B. L. Weber, W. R. Sellers, R. Schlegel, J. A. Wargo, W. C. Hahn, L. A. Garraway, COT drives resistance to RAF inhibition through MAP kinase pathway reactivation. *Nature* **468**, 968–972 (2010).
33. R. A. Lindquist, K. A. Ottina, D. B. Wheeler, P. P. Hsu, C. C. Thoreen, D. A. Guertin, S. M. Ali, S. Sengupta, Y. D. Shaul, M. R. Lamprecht, K. L. Madden, A. R. Papallo, T. R. Jones, D. M. Sabatini, A. E. Carpenter, Genome-scale RNAi on living-cell microarrays identifies novel regulators of *Drosophila melanogaster* TORC1–S6K pathway signaling. *Genome Res.* **21**, 433–446 (2011).
34. J. A. Engelman, K. Zejnullahu, T. Mitsudomi, Y. Song, C. Hyland, J. O. Park, N. Lindeman, C. M. Gale, X. Zhao, J. Christensen, T. Kosaka, A. J. Holmes, A. M. Rogers, F. Cappuzzo, T. Mok, C. Lee, B. E. Johnson, L. C. Cantley, P. A. Janne, MET amplification leads to gefitinib resistance in lung cancer by activating ERBB3 signaling. *Science* **316**, 1039–1043 (2007).
35. D. H. Kim, D. D. Sarbassov, S. M. Ali, J. E. King, R. R. Latek, H. Erdjument-Bromage, P. Tempst, D. M. Sabatini, mTOR interacts with raptor to form a nutrient-sensitive complex that signals to the cell growth machinery. *Cell* **110**, 163–175 (2002).
36. M. W. Karaman, S. Herrgard, D. K. Treiber, P. Gallant, C. E. Atteridge, B. T. Campbell, K. W. Chan, P. Ciceri, M. I. Davis, P. T. Edeen, R. Faraoni, M. Floyd, J. P. Hunt, D. J. Lockhart, Z. V. Milanov, M. J. Morrison, G. Pallares, H. K. Patel, S. Pritchard, L. M. Wodicka, P. P. Zarrinkar, A quantitative analysis of kinase inhibitor selectivity. *Nat. Biotechnol.* **26**, 127–132 (2008).
37. J. Tsai, J. T. Lee, W. Wang, J. Zhang, H. Cho, S. Mamo, R. Bremer, S. Gillette, J. Kong, N. K. Haass, K. Sproesser, L. Li, K. S. Smalley, D. Fong, Y. L. Zhu, A. Marimuthu,

H. Nguyen, B. Lam, J. Liu, I. Cheung, J. Rice, Y. Suzuki, C. Luu, C. Settachatgul, R. Shellooe, J. Cantwell, S. H. Kim, J. Schlessinger, K. Y. Zhang, B. L. West, B. Powell, G. Habets, C. Zhang, P. N. Ibrahim, P. Hirth, D. R. Artis, M. Herlyn, G. Bollag, Discovery of a selective inhibitor of oncogenic B-Raf kinase with potent antimelanoma activity. *Proc. Natl. Acad. Sci. U.S.A.* **105**, 3041–3046 (2008).
38. G. Bollag, P. Hirth, J. Tsai, J. Zhang, P. N. Ibrahim, H. Cho, W. Spevak, C. Zhang, Y. Zhang, G. Habets, E. A. Burton, B. Wong, G. Tsang, B. L. West, B. Powell, R. Shellooe, A. Marimuthu, H. Nguyen, K. Y. Zhang, D. R. Artis, J. Schlessinger, F. Su, B. Higgins, R. Iyer, K. D'Andrea, A. Koehler, M. Stumm, P. S. Lin, R. J. Lee, J. Grippo, I. Puzanov, K. B. Kim, A. Ribas, G. A. McArthur, J. A. Sosman, P. B. Chapman, K. T. Flaherty, X. Xu, K. L. Nathanson, K. Nolop, Clinical efficacy of a RAF inhibitor needs broad target blockade in *BRAF*-mutant melanoma. *Nature* **467**, 596–599 (2010).
39. K. T. Flaherty, I. Puzanov, K. B. Kim, A. Ribas, G. A. McArthur, J. A. Sosman, P. J. O'Dwyer, R. J. Lee, J. F. Grippo, K. Nolop, P. B. Chapman, Inhibition of mutated, activated BRAF in metastatic melanoma. *N. Engl. J. Med.* **363**, 809–819 (2010).
40. D. B. Solit, L. A. Garraway, C. A. Pratilas, A. Sawai, G. Getz, A. Basso, Q. Ye, J. M. Lobo, Y. She, I. Osman, T. R. Golub, J. Sebolt-Leopold, W. R. Sellers, N. Rosen, BRAF mutation predicts sensitivity to MEK inhibition. *Nature* **439**, 358–362 (2006).
41. A. Birmingham, L. M. Selfors, T. Forster, D. Wrobel, C. J. Kennedy, E. Shanks, J. Santoyo-Lopez, D. J. Dunican, A. Long, D. Kelleher, Q. Smith, R. L. Beijersbergen, P. Ghazal, C. E. Shamu, Statistical methods for analysis of high-throughput RNA interference screens. *Nat. Methods* **6**, 569–575 (2009).
42. C. M. Emery, K. G. Vijayendran, M. C. Zipser, A. M. Sawyer, L. Niu, J. J. Kim, C. Hatton, R. Chopra, P. A. Oberholzer, M. B. Karpova, L. E. MacConaill, J. Zhang, N. S. Gray, W. R. Sellers, R. Dummer, L. A. Garraway, MEK1 mutations confer resistance to MEK and B-RAF inhibition. *Proc. Natl. Acad. Sci. U.S.A.* **106**, 20411–20416 (2009).
43. J. W. Lee, Y. H. Soung, S. H. Seo, S. Y. Kim, C. H. Park, Y. P. Wang, K. Park, S. W. Nam, W. S. Park, S. H. Kim, J. Y. Lee, N. J. Yoo, S. H. Lee, Somatic mutations of *ERBB2* kinase domain in gastric, colorectal, and breast carcinomas. *Clin. Cancer Res.* **12**, 57–61 (2006).
44. Cancer Genome Atlas Research Network, Comprehensive genomic characterization defines human glioblastoma genes and core pathways. *Nature* **455**, 1061–1068 (2008).
45. R. Nazarian, H. Shi, Q. Wang, X. Kong, R. C. Koya, H. Lee, Z. Chen, M. K. Lee, N. Attar, H. Sazegar, T. Chodon, S. F. Nelson, G. McArthur, J. A. Sosman, A. Ribas, R. S. Lo, Melanomas acquire resistance to B-RAF(V600E) inhibition by RTK or N-RAS upregulation. *Nature* **468**, 973–977 (2010).
46. J. Villanueva, A. Vultur, J. T. Lee, R. Somasundaram, M. Fukunaga-Kalabis, A. K. Cipolla, B. Wubbenhorst, X. Xu, P. A. Gimotty, D. Kee, A. E. Santiago-Walker, R. Letrero, K. D'Andrea, A. Pushparajan, J. E. Hayden, K. D. Brown, S. Laquerre, G. A. McArthur, J. A. Sosman, K. L. Nathanson, M. Herlyn, Acquired resistance to BRAF inhibitors mediated by a RAF kinase switch in melanoma can be overcome by cotargeting MEK and IGF-1R/PI3K. *Cancer Cell* **18**, 683–695 (2010).
47. K. P. Hoeflich, S. Herter, J. Tien, L. Wong, L. Berry, J. Chan, C. O'Brien, Z. Modrusan, S. Seshagiri, M. Lackner, H. Stern, E. Choo, L. Murray, L. S. Friedman, M. Belvin, Antitumor efficacy of the novel RAF inhibitor GDC-0879 is predicted by $BRAF^{V600E}$ mutational status and sustained extracellular signal-regulated kinase/mitogen-activated protein kinase pathway suppression. *Cancer Res.* **69**, 3042–3051 (2009).
48. T. C. Yeh, V. Marsh, B. A. Bernat, J. Ballard, H. Colwell, R. J. Evans, J. Parry, D. Smith, B. J. Brandhuber, S. Gross, A. Marlow, B. Hurley, J. Lyssikatos, P. A. Lee, J. D. Winkler, K. Koch, E. Wallace, Biological characterization of ARRY-142886 (AZD6244), a potent, highly selective mitogen-activated protein kinase kinase 1/2 inhibitor. *Clin. Cancer Res.* **13**, 1576–1583 (2007).
49. N. Thompson, J. Lyons, Recent progress in targeting the Raf/MEK/ERK pathway with inhibitors in cancer drug discovery. *Curr. Opin. Pharmacol.* **5**, 350–356 (2005).
50. C. C. Thoreen, S. A. Kang, J. W. Chang, Q. Liu, J. Zhang, Y. Gao, L. J. Reichling, T. Sim, D. M. Sabatini, N. S. Gray, An ATP-competitive mammalian target of rapamycin inhibitor reveals rapamycin-resistant functions of mTORC1. *J. Biol. Chem.* **284**, 8023–8032 (2009).
51. S. M. Maira, F. Stauffer, J. Brueggen, P. Furet, C. Schnell, C. Fritsch, S. Brachmann, P. Chène, A. De Pover, K. Schoemaker, D. Fabbro, D. Gabriel, M. Simonen, L. Murphy, P. Finan, W. Sellers, C. Garcia-Echeverria, Identification and characterization of NVP-BEZ235, a new orally available dual phosphatidylinositol 3-kinase/mammalian target of rapamycin inhibitor with potent in vivo antitumor activity. *Mol. Cancer Ther.* **7**, 1851–1863 (2008).
52. C. Montagut, S. V. Sharma, T. Shioda, U. McDermott, M. Ulman, L. E. Ulkus, D. Dias-Santagata, H. Stubbs, D. Y. Lee, A. Singh, L. Drew, D. A. Haber, J. Settleman, Elevated CRAF as a potential mechanism of acquired resistance to BRAF inhibition in melanoma. *Cancer Res.* **68**, 4853–4861 (2008).
53. A. Subramanian, P. Tamayo, V. K. Mootha, S. Mukherjee, B. L. Ebert, M. A. Gillette, A. Paulovich, S. L. Pomeroy, T. R. Golub, E. S. Lander, J. P. Mesirov, Gene set enrichment analysis: A knowledge-based approach for interpreting genome-wide expression profiles. *Proc. Natl. Acad. Sci. U.S.A.* **102**, 15545–15550 (2005).
54. A. M. Aronov, Q. Tang, G. Martinez-Botella, G. W. Bemis, J. Cao, G. Chen, N. P. Ewing, P. J. Ford, U. A. Germann, J. Green, M. R. Hale, M. Jacobs, J. W. Janetka, F. Maltais, W. Markland, M. N. Namchuk, S. Nanthakumar, S. Poondru, J. Straub, E. ter Haar, X. Xie, Structure-guided design of potent and selective pyrimidylpyrrole inhibitors of extracellular signal-regulated kinase (ERK) using conformational control. *J. Med. Chem.* **52**, 6362–6368 (2009).
55. M. Karin, Y. Ben-Neriah, Phosphorylation meets ubiquitination: The control of NF-κB activity. *Annu. Rev. Immunol.* **18**, 621–663 (2000).
56. W. M. Lin, A. C. Baker, R. Beroukhim, W. Winckler, W. Feng, J. M. Marmion, E. Laine, H. Greulich, H. Tseng, C. Gates, F. S. Hodi, G. Dranoff, W. R. Sellers, R. K. Thomas, M. Meyerson, T. R. Golub, R. Dummer, M. Herlyn, G. Getz, L. A. Garraway, Modeling genomic diversity and tumor dependency in malignant melanoma. *Cancer Res.* **68**, 664–673 (2008).
57. R. S. Lokey, Forward chemical genetics: Progress and obstacles on the path to a new pharmacopoeia. *Curr. Opin. Chem. Biol.* **7**, 91–96 (2003).
58. A. B. Parsons, A. Lopez, I. E. Givoni, D. E. Williams, C. A. Gray, J. Porter, G. Chua, R. Sopko, R. L. Brost, C. H. Ho, J. Wang, T. Ketela, C. Brenner, J. A. Brill, G. E. Fernandez, T. C. Lorenz, G. S. Payne, S. Ishihara, Y. Ohya, B. Andrews, T. R. Hughes, B. J. Frey, T. R. Graham, R. J. Andersen, C. Boone, Exploring the mode-of-action of bioactive compounds by chemical-genetic profiling in yeast. *Cell* **126**, 611–625 (2006).
59. S. Zhang, W. C. Huang, P. Li, H. Guo, S. B. Poh, S. W. Brady, Y. Xiong, L. M. Tseng, S. H. Li, Z. Ding, A. A. Sahin, F. J. Esteva, G. N. Hortobagyi, D. Yu, Combating trastuzumab resistance by targeting SRC, a common node downstream of multiple resistance pathways. *Nat. Med.* **17**, 461–469 (2011).
60. V. C. Gray-Schopfer, M. Karasarides, R. Hayward, R. Marais, Tumor necrosis factor-α blocks apoptosis in melanoma cells when BRAF signaling is inhibited. *Cancer Res.* **67**, 122–129 (2007).
61. T. G. Bivona, H. Hieronymus, J. Parker, K. Chang, M. Taron, R. Rosell, P. Moonsamy, K. Dahlman, V. A. Miller, C. Costa, G. Hannon, C. L. Sawyers, FAS and NF-κB signalling modulate dependence of lung cancers on mutant EGFR. *Nature* **471**, 523–526 (2011).
62. F. Li, G. Sethi, Targeting transcription factor NF-κB to overcome chemoresistance and radioresistance in cancer therapy. *Biochim. Biophys. Acta* **1805**, 167–180 (2010).
63. P. J. Perrin, J. H. Maldonado, T. A. Davis, C. H. June, M. K. Racke, CTLA-4 blockade enhances clinical disease and cytokine production during experimental allergic encephalomyelitis. *J. Immunol.* **157**, 1333–1336 (1996).
64. J. Yuan, S. Gnjatic, H. Li, S. Powel, H. F. Gallardo, E. Ritter, G. Y. Ku, A. A. Jungbluth, N. H. Segal, T. S. Rasalan, G. Manukian, Y. Xu, R. A. Roman, S. L. Terzulli, M. Heywood, E. Pogoriler, G. Ritter, L. J. Old, J. P. Allison, J. D. Wolchok, CTLA-4 blockade enhances polyfunctional NY-ESO-1 specific T cell responses in metastatic melanoma patients with clinical benefit. *Proc. Natl. Acad. Sci. U.S.A.* **105**, 20410–20415 (2008).
65. J. S. Economou, M. Hoban, J. D. Lee, R. Essner, S. Swisher, W. McBride, D. B. Hoon, D. L. Morton, Production of tumor necrosis factor α and interferon γ in interleukin-2-treated melanoma patients: Correlation with clinical toxicity. *Cancer Immunol. Immunother.* **34**, 49–52 (1991).
66. A. Boni, A. P. Cogdill, P. Dang, D. Udayakumar, C. N. J. Njauw, C. M. Sloss, C. R. Ferrone, K. T. Flaherty, D. P. Lawrence, D. E. Fisher, H. Tsao, J. A. Wargo, Selective $BRAF^{V600E}$ inhibition enhances T-cell recognition of melanoma without affecting lymphocyte function. *Cancer Res.* **70**, 5213–5219 (2010).
67. C. L. Chaffer, I. Brueckmann, C. Scheel, A. J. Kaestli, P. A. Wiggins, L. O. Rodrigues, M. Brooks, F. Reinhardt, Y. Su, K. Polyak, L. M. Arendt, C. Kuperwasser, B. Bierie, R. A. Weinberg, Normal and neoplastic nonstem cells can spontaneously convert to a stem-like state. *Proc. Natl. Acad. Sci. U.S.A.* **108**, 7950–7955 (2011).
68. R. A. Irizarry, B. Hobbs, F. Collin, Y. D. Beazer-Barclay, K. J. Antonellis, U. Scherf, T. P. Speed, Exploration, normalization, and summaries of high density oligonucleotide array probe level data. *Biostatistics* **4**, 249–264 (2003).
69. Z. Jagani, E. L. Mora-Blanco, C. G. Sansam, E. S. McKenna, B. Wilson, D. Chen, J. Klekota, P. Tamayo, P. T. L. Nguyen, M. Tolstorukov, P. J. Park, Y. J. Cho, K. Hsiao, S. Buonamici, S. L. Pomeroy, J. P. Mesirov, H. Ruffner, T. Bouwmeester, S. J. Luchansky, J. Murtie, J. F. Kelleher, M. Warmuth, W. R. Sellers, C. W. M. Roberts, M. Dorsch, Loss of the tumor suppressor Snf5 leads to aberrant activation of the Hedgehog-Gli pathway. *Nat. Med.* **16**, 1429–1433 (2010).
70. P. Tamayo, Y. J. Cho, A. Tsherniak, H. Greulich, L. Ambrogio, N. Schouten-van Meeteren, T. Zhou, A. Buxton, M. Kool, M. Meyerson, S. L. Pomeroy, J. P. Mesirov, Predicting relapse in patients with medulloblastoma by integrating evidence from clinical and genomic features. *J. Clin. Oncol.* **29**, 1415–1423 (2011).
71. T. Cover, J. Thomas, *Elements of Information Theory* (John Wiley & Sons, Hoboken, NJ, 2006).
72. D. W. Scott, *Multivariate Density Estimation: Theory, Practice, and Visualization* (John Wiley & Sons, Hoboken, NJ, 1992).
73. L. Ming, C. Xin, L. Xin, M. Bin, P. M. B. Vitanyi, The similarity metric. *IEEE Trans. Inform. Theory* **50**, 3250–3264 (2004).
74. A. Kraskov, H. Stogbauer, R. G. Andrzejak, P. Grassberger, Hierarchical clustering using mutual information. *Europhys. Lett.* **70**, 278–286 (2005).

Acknowledgments: We thank D. Wheeler, R. Lindquist, Y. Shaul, L. Bar-Peled, K. Ottina, G. Underhill, S. Gopal, A. Derr, K. Saha, K. B. Wood, and the members of the Sabatini lab for helpful discussions and technical assistance; J. Grenier, S. Silver, O. Alkan, C. Nguyen, and the members of the Broad Institute RNAi Platform for assistance in producing and titering lentiviruses; H. Greulich for contributing mutant ORF constructs to the screening library; T. Holway and T. Sullivan (Aushon BioSystems) for assistance with microarray printing; T. DiCesare for assistance with illustrations; P. Wisniewski for assistance with flow cytometry; and members of the Broad Institute/Novartis CCLE for contributing cell line mutation, gene expression, and pharmacological sensitivity data. **Funding:** This work was supported by a Scientific Planning and Allocation of Resources Committee grant from the Broad Institute (D.M.S.), NIH grant 5R01-CA129105 (D.M.S.), and a grant from the Novartis Institutes for Biomedical Research (L.A.G.). K.C.W. is the recipient of an NIH Ruth L. Kirschstein National Research Service Award and a Misrock Fund Postdoctoral Fellowship through the Koch Institute for Integrative Cancer Research at the Massachusetts Institute of Technology. D.M.S. is an investigator of the Howard Hughes Medical Institute. **Author contributions:** K.C.W., D.E.R., and D.M.S. designed and created the MicroSCALE screening platform. J.S.B. and W.C.H. provided the Kinome ORF library. D.E.R. oversaw lentivirus production. L.A.G. led the acquisition of cell line mutation, gene expression, and pharmacological sensitivity data. J.P.M., O.B.B., and P.T. designed methodologies for gene set projection and gene set to drug profile matching. D.J.K. and P.T. performed gene set enrichment and profile matching analyses. All authors contributed to the design of experiments and analysis of results. K.C.W. performed all experiments and wrote the manuscript, and all authors provided editorial input. **Competing interests:** K.C.W., D.E.R., and D.M.S. are inventors on a U.S. patent application describing the MicroSCALE platform. The Broad Institute along with the Whitehead Institute for Biomedical Research is applying for a patent for the lentiviral spotted array technology. L.A.G. is a consultant for Novartis Pharmaceuticals and Millennium/Takeda Pharmaceuticals and is a consultant and shareholder of Foundation Medicine. The authors declare that they have no additional competing financial interests. **Data and materials availability:** Gene expression, genomic characterization, and pharmacological sensitivity data used for this study are available from http://www.broadinstitute.org/ccle/home.

Submitted 17 October 2011
Accepted 25 April 2012
Final Publication 15 May 2012
10.1126/scisignal.2002612
Citation: K. C. Wood, D. J. Konieczkowski, C. M. Johannessen, J. S. Boehm, P. Tamayo, O. B. Botvinnik, J. P. Mesirov, W. C. Hahn, D. E. Root, L. A. Garraway, D. M. Sabatini, MicroSCALE screening reveals genetic modifiers of therapeutic response in melanoma. *Sci. Signal.* **5**, rs4 (2012).